Non-destructive quantification of water gradient in sludge composting with Magnetic Resonance Imaging

F.P. Duval, S. Quellec, A. Trémier, C. Druilhe, François Mariette

Author-produced version of the article published in Waste Management, 2010, 30, 4. 610-619.
Original publication available at www.sciencedirect.com – doi:10.1016/j.wasman.2009.09.045

Non-Destructive Quantification of Water Gradient in Sludge Composting with Magnetic Resonance Imaging

F.P. Duval[1,3], S. Quellec[1,3], A. Trémier[2,3], C. Druilhe[2,3], F. Mariette[1,3,*]

1-Cemagref, UR TERE, 17 Avenue de Cucillé, CS 64427, F-35044 Rennes, France.

2-Cemagref, UR GERE, F-35044 Rennes, France.

3-Université européenne de Bretagne, France.

* Corresponding author. Tel.: +33 2 23 48 21 21; Fax: +33 2 23 48 21 15; E-mail address: francois.mariette@cemagref.fr

Abstract

Sludge from a slaughterhouse wastewater plant, and mixtures of bulking agent (crushed wood pallet) and sludge were studied by Nuclear Magnetic Resonance (NMR). The NMR spin-spin relaxation (T_2) and spin-lattice relaxation (T_1) signals for sludge, wet crushed wood pallet and mixtures of sludge and bulking agent were decomposed into three relaxation time components. Each relaxation time component was explained by a non-homogeneous water distribution on a microscopic length scale and by the porosity of the material. For all samples, the T_2 relaxation time value of each component was directly related to the dry matter content. The addition of wet crushed wood to sludge induced a decrease in the relaxation time, explained by water transfer between the sludge and the wood.

Magnetic Resonance Imaging (MRI) and respirometric measurements were performed on sludge and wood mixtures. MR images of the mixtures were successfully obtained at different biodegradation states. Based on specific NMR measurements in an identified area located in the MRI cells, the results showed that grey levels of MR images reflected dry matter content. This preliminary study showed that MRI would be a powerful tool to measure water distribution in sludge and bulking agent mixtures and highlights the potential of this technique to increase the understanding of sludge composting.

Keywords: NMR, MRI, relaxation, compost, biodegradability, moisture content, bulking agent, sludge

1. Introduction

Treatment of wastewater is an important issue in western countries and research is currently being undertaken to investigate the elimination or re-use of residual sludge at better cost, including composting of wastewater sludge. In order to do so, sludge needs to be mixed with a bulking agent which creates a porous matrix. Proportions of sludge and bulking agent are chosen so that sludge covers the bulking agent with a thin layer, and then micro-organisms in the sludge are sufficiently aerated to consume the available biodegradable organic matter. During sludge composting treatment, the active biodegradation takes place in three to four weeks, followed by several months of maturation (Gupta, 2008). Selection of an initial waste recipe with optimal physical and biochemical parameters is essential to create an environment conducive to high microbial growth and activity, and then to shorten and improve the biodegradation in the active phase (Haug, 1993; Agnew, 2003). Some of the important physical parameters for this waste recipe are water content, air porosity and specific surface area.

Research on composting is often focused on overall understanding of the biodegradation phenomena, i.e. on a macro-scale. All the parameters of biodegradation such as oxygen consumption, bacteria activity, porosity and moisture content are averaged, and little is known regarding the influence of local behaviour of the physical parameters on overall biodegradation. Since solid wastes are very heterogeneous, better understanding of water content, porosity and specific surface spatial distribution is needed, and Magnetic Resonance Imaging (MRI) could help to fill this gap. Indeed, most of the common techniques to measure physical parameters can not be applied along the composting process because they are invasive or destructive. Moisture measurements need sampling and drying. Classic porosity measurement implies to fill the porous volume with a liquid (Annan, 1998), which is destructive for the sample. Pycnometry is a non destructive method but results directly depend

on the applied pressure leading to the measurement of total air space (TAS) or only free air space (FAS) (Su, 2006). Measurement of the specific surface is not easier. The direct measurement technique through gaseous absorption (BET) used by Palmowski et al. (Palmowski, 2003) can only be applied after drying the waste. On the contrary, MRI is non-destructive and non-invasive and thus makes it possible to follow the evolution of samples over time. MRI is well known for its medical applications, but it has been used in other fields including the wood industry (Muller, 2002), study of bacterial chemotaxis (Sherwood, 2003; Olson, 2004), chemical engineering (Mantle, 2003), civil engineering (Faure, 2005), fluid mechanics (Bonn, 2008), pharmaceutical science (Richardson, 2005) and food science (Hills, 1998; Butz, 2005). In an MRI experiment, the volume in which the signal is collected is called a voxel, and its typical order of magnitude is the cubic millimetre. Voxel intensity is a function of local proton density and of their respective spin-lattice (T_1) and spin-spin (T_2) relaxation times. Proton density is proportional to the amount of material containing protons. In most materials, water is the main constituent related to proton density. Consequently, the grey level intensity of a voxel may be related to water content or air content (*i.e.* porosity). Indeed when the voxel size is larger than the pore size the porosity is directly related to the intensity of the MRI signal: the greater the quantity of gas, the lower the signal. This method has been used in food science to quantify the distribution of porosity during proving of dough (Grenier, 2003; Lucas, 2005). In the extreme case where the pore volume is much larger than the voxel size, the pore size can be measured. For example, air cavities have been detected and quantified in food products such as cheese (Mariette, 2004; 2006). In addition to the porous fraction, the specific surface area can be estimated if the resolution of the MR images is good enough.

Spin-lattice (T_1) and spin-spin (T_2) relaxation times are related to water content and also to material microstructure and to molecular structure (Brownstein, 1979; Belton, 1987; Hills,

1989b; a; Denisov, 2002). Several authors have used the T_2 and T_1 relaxation times as tracers of water content for the investigation of draining processes (Mariette, 2006) and rehydration processes (Ziegler, 2003).

The aim of this study was to evaluate the potential of the MRI technique in sludge composting to quantify the water distribution. . The first part of this report focuses on the description of the nuclear magnetic resonance (NMR) signals in sludge and in mixtures of sludge and bulking agent and their sensitivity to water content. The second part describes the preliminary results of MRI images from sludge and bulking agent mixture. The potential for determination of water content and measurement of local porosity by MRI is discussed.

2. Materials and Methods

2.1 Sludge and bulking agent

The sludge came from the biological activated sludge treatment of the wastewater from a slaughter-house. Iron chloride and a polymeric flocculent (PRAESTOL K133) were added to the sludge to induce flocculation and, after a decantation step, the sludge was dewatered using a press band. The collected sludge was stored frozen at -20°C in 1kg batches. Sludge was unfrozen before each experiment, initially in a refrigerator at 4°C and then at room temperature.

The dry matter (DM, measured by drying at 105°C until constant weight) in the sludge was 13.6% of total weight, with approximately 80% organic matter to DM. The exact quantity of living bacteria present in the sludge was unknown. Flocs of bacteria were observed using optical microscopy (data not shown). Sludges with higher dry matter content were prepared using a low pressure oven (34 Mb and 30°C). Mixtures of sludge and bulking agent were prepared by hand mixing the sludge with crushed wood pallet as bulking agent. The size of the wood chips considered was 8 to 12 mm. Wood was stored after drying at 80°C. Different

samples were then studied by NMR, i.e. the sludge without bulking agent, mixtures of wood and sludge, and a rehydrated wood sample (DM 45%). Since there is water transfer between sludge and dried wood after mixing, the saturated wood sample was prepared to mimic the contribution of the re-hydrated wood fraction in the mixture.

A combined experiment using MRI and respirometry was set up. Two large respirometric cells were prepared with 4.5 kg of sludge (wet) mixed with 2.5 kg of wood (dry mass ratio 1/4.1 g_{DM}/g_{DM}). The moisture content in both cells was approximately 56%. MRI measurements were performed at day 1, day 3 and day 27 of biodegradation. Samples were taken from these cells for NMR measurement and moisture analysis at 27 days.

2.2 Respirometry

Respirometry is a useful tool to assess microbial activity (Iannotti, 1994; Adani, 2001; Gea, 2004). The respirometric apparatus used in this study consisted of a 10 L airtight cylindrical reactor made of glass. Three to four kilos of precisely weighed material were introduced into the respirometric reactor on a 3 mm round mesh grid placed 70 mm above the cell bottom. An entering air flow rate of 65 L/h (compressed air) was applied throughout the experiments. Homogeneity of aeration of the entire sample was provided by means of the rapid recirculation of the exhaust gas in the cell (360 L/h). The entering and exhaust air streams were monitored for O_2 content using a paramagnetic O_2 gas analyser (MAHAIK Technology, Germany).

The apparatus was monitored for the main environmental factors influencing microbial activity, i.e. temperature and moisture. As shown on **Figure 1** the temperature of samples was held constant by placing each respirometric cell in a water-bath at 40°C, which is optimal for biodegradation activity (Tremier, 2005). The inlet air was preheated to 40°C using a copper tubular coil with a diameter of 10 mm, thickness of 2 mm and length of 2 m, submerged in the

141 water-bath. The sample temperatures were monitored by means of a Pt100 temperature probe
142 (OMNI Instrument, UK) inserted in the centre of the sample. For the moisture control, the
143 inflowing air was saturated by bubbling through two water-filled glass bottles immersed in
144 the water-bath. Moisture condensing in the exhaust air was collected in beakers above the
145 water-bath to prevent its return into the sample cell and its entrance into the gas analyser.
146
147
148
149 2.3 NMR measurements
150 All NMR measurements were performed with a 10 MHz Minispec Mq10 (Bruker,
151 Wissembourg, France). Typical 90° and 180° pulse durations were 14 µs and 32 µs,
152 respectively, with an 8 dB pulse attenuation. The temperature was fixed at 20°C. Spin-Spin
153 relaxation time (T_2) measurements were performed using a Carr Purcell Meiboom and Gill
154 (CPMG) sequence (Meiboom, 1958). Three thousand consecutive echoes were recorded with
155 a time spacing of 0.1 ms between the 90° and the first 180° pulse. Recycle delay and number
156 of scans were 2 s and 8 s, respectively. Spin-Lattice relaxation time (T_1) measurements were
157 performed using a saturation recovery (SR) sequence. Times between the two 90° pulses were
158 varied one hundred times from 5 ms to 2000 ms. The NMR signal was acquired 28 µs after
159 the second 90° pulse in order to detect only the longest relaxation components, *i.e*, the water
160 proton relaxation. Recycle delay and number of scans were 2 s and 8 s, respectively.
161
162 2.5 Calculation of NMR parameters
163 Relaxation curves were fitted using two different methods, the Maximum Entropy Method
164 (MEM) (Mariette, 1996), which provides a continuous distribution of relaxation components,
165 and the Levenberg-Marquardt algorithm, which allows discrete solution for the fitting (Table

Curve, Jandel) (Marquardt, 1963). Moreover, no assumptions regarding the number of relaxation times are necessary with MEM compared to the Levenberg-Marquardt algorithm method.

For the spin-spin relaxation decay signal, the equation used for fitting according to the Levenberg-Marquardt method was:

$$S(t)_{CPMG} = I_1 e^{-\frac{t}{T_{21}}} + I_2 e^{-\frac{t}{T_{22}}} + I_3 e^{-\frac{t}{T_{23}}} + c \qquad \text{Eq.1}$$

where $S(t)_{CPMG}$ is the intensity of the total relaxation signal (a.u.), t is the time of the relaxation process (ms), T_{2i} the spin-spin relaxation time of the component *i* (ms) and I_i the associated signal (a.u.). A constant c was added into the model in order to take into account change in the decay baseline.

Spin-Lattice relaxation curves were fitted with the Levenberg-Marquardt algorithm with the following equation:

$$S(t)_{SR} = I_1(1-\alpha e^{-\frac{t}{T_{11}}}) + I_2(1-\alpha e^{-\frac{t}{T_{12}}}) + I_3(1-\alpha e^{-\frac{t}{T_{13}}}) \qquad \text{Eq.2}$$

where $S(t)_{SR}$ is the intensity of the total relaxation signal (a.u.), t is the time of the relaxation process (ms), T_{1i} the spin-lattice relaxation time of the component *i* (ms) and I_i the associated signal (a.u.). A constant α was introduced to correct for imperfections in the 90° pulse.

2.6 MRI measurements

A 1.5 Tesla whole body MRI scanner (Magneton Avento Siemens, Erlangen, Germany) was used. The MR images were acquired with the standard spin echo sequence. Forty-five slices of 2 mm were recorded, the distance between the centres of two consecutive slices being 4 mm. The field of view was 220 mm x 220 mm for 256 x 256 pixel sampling. Echo time (T_E), repetition time (T_R) and pixel bandwidth were 8 ms, 1000 ms and 395 Hz/pixel, respectively.

The grey level intensity S_{ES} (a.u) within a voxel with a standard spin-echo sequence was given by the equation:

$$S_{ES} = I\left(1 - \beta e^{-\frac{T_R}{T_1}}\right) \times e^{-\frac{T_E}{T_2}} \quad \text{Eq.3}$$

with I the intensity related to the relaxation times T_1 and T_2 of the protons in the voxel. β is a parameter introduced to correct for imperfections in the 90° pulse. This equation assumed a single proton component with a single spin-spin relaxation and a single spin-lattice relaxation. In the case of multi-exponential behaviour, the grey level intensity would be a combination of the different relaxing components for both T_1 and T_2.

3. Results and discussion

3.1 NMR

Figure 2 shows typical CPMG (a) and SR (b) signals for two wood and sludge mixtures with dry matter of 24% and 70%. CPMG signal intensities decreased throughout the acquisition time t, according to equation 1. An increase in signal intensity was obtained for SR as expected from equation 2. The effects of water content on NMR parameters can be described from the two CPMG signals. Firstly, since the initial signal intensity was proportional to the sample proton content, and because water is one of the most abundant protonic molecules in our system, this explains the reduction in signal intensity from 3.7 to 2.2 a.u. observed between the two samples. Secondly, the water relaxation time is highly sensitive to water content. Indeed, T_2 relaxation was directly related to molecular mobility, i.e., the slower the molecular mobility the shorter the relaxation time (Belton, 1990). The relaxation time of a small molecule is thus always higher than the relaxation time of a large molecule. Moreover, the exchange between water protons and exchangeable protons from the molecule contained in the dry matter has to be taken into account for water. This exchange, known as chemical

exchange, is one of the most efficient mechanisms of water relaxation (Belton, 1987; Hills, 1989b; a; Belton, 1990; Denisov, 2002). Consequently, water relaxation is always sensitive to water content and its value decreases with water content, explaining the more rapid decrease in the CPMG signal observed for the driest sample. The same mechanisms are also involved in the T_1 relaxation from the Saturation Recovery NMR sequence. The intensity measured at 2 s was lower for the driest sample and the recovery of the signal (shorter T_1) was faster for the driest sample.

The spin-spin relaxation distributions (T_2) from MEM obtained from fitting the CPMG curve are presented in Figure 3. For all samples, two or three peaks were extracted from the signal according to the sample dry matter. Two mechanisms can be proposed to explain such multi-exponential relaxation behaviour. The first is based on the assumption of the chemical composition of the sample. For example, in the case of the water and fat mixture in an emulsion, a specific exponential can be attributed to each phase, *i.e.* water and fat (Duval, 2006). However, since our samples were mainly composed of water, this hypothesis did not hold. The second mechanism is based on the sample microstructure which may induce non-homogeneous water distribution on a microscopic length scale. Indeed, when water exchange by diffusion between different compartments is slow compared to the relaxation time value, the averaging effect is not sufficient to yield a single relaxation time value, and several peaks are observed for the water relaxation. This multi-exponential relaxation for water has already been reported for many samples which exhibited restriction to the water diffusion. For example three peaks have been reported from the relaxation decay curve of vegetable tissues. These peaks were attributed to water in the vacuole, in the cytoplasm and in the cell wall, respectively (Snaar, 1992; Van Dusschoten, 1995; Duval, 2005; Musse, 2009). This mechanism therefore seems the most relevant to explain the multi-exponential behaviour of the relaxation.

239 For the sludge, depending on the dry matter, two or three peaks were extracted from the signal
240 (Figure 3-a). Their T_2 values covered a range from 5 to 60 ms. The sludge was composed of
241 flocculated bacteria which induced heterogeneity in the water distribution. Indeed, water was
242 always present in bacteria, in and around the flocs. Since water protons are thus in three
243 different compartments, it is tempting to associate each relaxation time with a water
244 compartment. Granular sludges have already been studied by NMR (Lens, 1997; Lens, 1999),
245 and a relaxing agent was used to lower the proton relaxation times in the solution. Relaxation
246 times of 10-15 ms and 30 ms were attributed to methanogenic (Lens, 1999) and sulfidogenic
247 bacteria (Lens, 1997), respectively. Water in the granular matrix had a relaxation time of 40-
248 100 ms (Lens, 1999). According to these results, the first peak could be related to the bacteria
249 and the second to the water around the bacteria (Figure 3-a). However, a water proton from
250 the solution could well contribute to the first or the second peak. Since no peak was found
251 with a value close to the free water value (1.5-3 s), this means that there were some molecules
252 in the sludge solution that lowered the overall relaxation of the proton of this compartment.
253 The polymer added for the flocculation could explain the decrease in the water relaxation
254 time, but the effect of the iron chloride (used to dehydrate the sludge) has also to be taken into
255 account.
256 Wood relaxation is well documented in the literature (Hsi, 1977; Menon, 1987; Araujo, 1992;
257 Araujo, 1994; Hartley, 1994; Xu, 1996). Three main relaxation times were found related to
258 water in cell wall fibrils (fast T_2), water in the ray and late wood tracheid lumens (medium T_2)
259 and water in early wood tracheid lumens (fast T_2). Above the fiber saturation point (FSP),
260 wood relaxation times are relatively constant over a wide range of water content (Menon,
261 1987). Below FSB, the relaxation times are a function of water content. The wood used in this
262 study had a similar relaxation time distribution (Figure 3-b) as that reported for Western Red
263 Cedar sapwood (Menon, 1987). At a water content of 55%, the mean relaxation times were 10

ms, 35 ms and 115 ms. The last two peaks were broad. Wood relaxation is sensitive to cell size and wood species. Since the wood used in this study was heterogeneous in origin, this would explain the peak shapes.

In a wood and sludge mixture there was water equilibrium between the two. After mixing, the sludge tended to loose water and the wood tended to gain water. Three typical relaxation distributions of wood and sludge mixtures are presented in Figure 3-c. The dry matter mixtures were 24%, 50% and 71%, respectively. Two or three peaks could be seen, the first being narrow (in the range of 0-10 ms), and the second peak broad, the range becoming larger with the increase in water content. Eventually, two broad peaks could be seen for the wettest samples. For the driest samples, the wood FSP was most probably not reached since no relaxation times were found above 40 ms. When the samples became wetter, the wood water content must have been above the FSP. Water filled the wood cells and then the relaxation time distribution could become broader. One important result in this study was that most of the T_2 relaxation distributions for wood and sludge were in the same range. Thus it was not possible to distinguish specific NMR signals from the sludge and the wood in the wood-sludge relaxation distribution.

Using the Levenberg-Marquardt algorithm to fit the T_2 relaxation decay curves, the smallest residues were obtained with a three component fitting equation (equation 1). The three T_2 values were consistent with the T_2 distribution discussed above. Relaxation rates ($R_2 = 1/T2$) for the three components are plotted on Figure 4 for sludge samples (a) and for sludge and wood mixtures (b). For all samples, a constant decrease was observed with the increase in water mass over dry matter mass. Moreover, the variation in relaxation rate was the same for the three components. This demonstrates that all fractions were in equilibrium and were affected by the dehydration process in the same way, despite the micro heterogeneity in the

289 water distribution in the sample. It should be noted that the same variation was observed for
290 sludge dehydrated by air drying and by exchange with dry wood. These results confirm that
291 the main effect on the water relaxation rate in the two samples was the dry matter content.
292 Spin-lattice relaxation times (T_1) were measured for wood and sludge mixtures. As for the
293 spin-spin relaxation curves, the spin-lattice relaxation curves were fitted with MEM and the
294 Levenberg-Marquardt algorithm (equation 2). The MEM distributions were composed of two
295 or three peaks (Figure 5-a), the first peak being narrow (range 5-20 ms), the other peaks being
296 broad (ranging from 15 ms to 250 ms). The Levenberg-Marquardt algorithm had the smallest
297 residues for the three components. The difference between the two fitting methods obtained
298 for some mixtures (two components from MEM and three from the discrete method) is
299 explained by the wide distribution of the second peak. Indeed, this effect is known to induce
300 discrepancies between the fitting methods (Mariette, 1996). The second peak obtained by
301 MEM was decomposed into two discrete T_1 values with the discrete method. As for R_2, a
302 linear relationship in a log-log plot was observed between the spin-lattice relaxation rate R_1
303 and the water mass over dry matter mass (Figure 5-b). Moreover, this relationship was
304 obtained for the three components. Only the T_2 sensitivity to water content will be considered
305 for the following MRI measurement.
306
307 3.2 MRI
308 Two experimental cells were scanned with the whole body MRI scanner at different periods
309 of biodegradation. In the mean time, the cells were monitored for biodegradation through
310 respirometry measurements (Figure 6). Indeed, oxygen consumption is a good indicator of
311 sludge biodegradation. The respirometric profiles obtained, that were similar for the two cells,
312 are typical. The oxygen uptake rate increased quickly due to biodegradation of the most easily
313 biodegradable substrate. Then, when all this matter had been degraded, a break in the

314 exponential growth was observed. The oxygen consumption rate then decreased until all the
315 biodegradable substrates had completely disappeared. During this decrease, the slowly
316 biodegradable organic matter was hydrolysed before being consumed by micro-organisms.
317 After 27 days, consumption rate returned to ground state and respirometric study could then
318 be stopped (Tremier, 2005; Berthe, 2007).
319 Both respirometric cells were thus scanned at D0 before biodegradation, then cell 1 at D3
320 after the biodegradation peak, and finally cell 2 at D27 when biodegradation was low and
321 constant. Examples of MR images at D0, D3 and D27 are presented in Figure 7. Images (a)
322 and (b) and images (c) and (d) were taken at the same location in cell 1 and in cell 2,
323 respectively. At D0, cell 1 (Figure 7-a) and cell 2 (Figure 7-c) images were similar: no
324 differences between the MR images for the two cells could be seen. The wet pieces of wood
325 covered with sludge were clearly visible. The black areas were the air space between the
326 bulking agents. The contrast in the image will allow to implement image segmentation
327 method to compute the inter porosity and the specific surface area. For larger pieces of wood,
328 the edges of the wood tended to be more intense than the centres, showing that the water had
329 not yet fully hydrated the centres of the wood. NMR relaxation experiments showed that this
330 process required at least 10h (data not shown). After 3 days, the edge effect was less visible
331 for cell 1 and the wood chips were even better defined (Figure 7-b). MR images of cell 2
332 taken after 27 days were highly contrasted. The MR image (Figure 7-d) showed two distinct
333 areas. Very low signal intensity was detected at the bottom of the image, compared with a
334 high level signal intensity at the top. This was due to the fact that cell 2 became highly
335 heterogeneous in water content in 27 days. The low intensity area had dry matter content of
336 around 60-70%. The intensity of the mixture signal was too low to be fully detected with
337 MRI. The other area had a dry matter content of around 25%, which demonstrated water
338 transfer in the cell. At D3, the water content in cell 1 also began to be inhomogeneous, but to

339 a lesser extent. The average dry matter content was 44%, two percent less than at D0. The
340 contrast between D3 and D27 was thus due to the difference in dry matter content.
341 MRI images were obtained with a spin echo sequence, the grey level intensities being a
342 function of both relaxation times (T_1, T_2) and the amount of water (see eq.3). Since the
343 repetition time, T_R, was 1 s and the largest spin-lattice relaxation time (T_1) found for the
344 wettest wood and sludge mixture was 250 ms, then in equation 3, $\left(1-\beta e^{-\frac{T_R}{T_1}}\right) \sim 1$. Thus, the
345 MR images were not T_1 weighted. Equation 3 can be rewritten for the three components as:

346 $$S_{ES} = I_1 e^{-\frac{T_E}{T_{21}}} + I_2 e^{-\frac{T_E}{T_{22}}} + I_3 e^{-\frac{T_E}{T_{23}}} \quad \text{Eq.4}$$

347

348 Since the intensity of each component I_i and the three T_2 relaxation times were strongly
349 dependent on the water content of the sample, the global signal intensity should consequently
350 also be directly related to water content in the mixture. This direct relationship was checked
351 by taking samples from cell 1 at D3 and from cell 2 at D27 at different heights in the cells
352 where MR images showed inhomogeneity. NMR and moisture content measurements were
353 performed on these samples. Signal intensities at 8 ms were extracted from the NMR CPMG
354 experiments and plotted against dry matter (Figure 8). As expected, the intensities decreased
355 with dry mater content. Despite the biological activity during the 27 days of storage, no
356 biodegradation effect was observed. The results provide evidence that the effect of biological
357 activity on the NMR signal of wood and sludge mixtures is negligible with regard to dry
358 matter content. The decay was non-linear. Indeed, with an 8 ms echo time, the multi-
359 exponential behaviour introduced a weighting from the different components. We
360 demonstrated that the grey levels of the MRI images were directly related to dry matter
361 content when the water content was above 40-30%. Below this value the signal was too low
362 to be detected with this MRI protocol.

363 MRI has been used previously to monitor wood decay by fungus (Muller, 2002): indeed
364 biological activity means a local increase in water content, which leads to a local change in
365 relaxation times and intensities. In this experiment, respirometry showed that biodegradation
366 occurred and both the NMR measurements and the MR images showed changes in the dry
367 matter content. MR images gave 3D representation of the heterogeneity of dry matter content
368 in the cells after 27 days of biodegradation (Figure 9). Heterogeneity was both vertical and
369 horizontal. Biodegradation may contribute to the heterogeneity of the dry matter, but the main
370 cause seems to be related to the cell design. The dried area is above the tube where air flows
371 into the cell. The air rate must be too fast and then has a drying effect. The humid area is
372 located under the tube where air flows out of the cell (Figure 2). Even with the water trap,
373 some water seems to condense in this tube and then drops to the wood and sludge mixture.
374 Thus, these MR images cannot be taken as proof of biodegradation activity. Nevertheless,
375 they will be used to improve the design of the respiratory cell.

376 **4. Conclusion**

377 We have shown that the NMR water relaxation for wood and sludge exhibited a multi-
378 exponential relaxation time behaviour which can be explained by the microstructure of the
379 matrix. Moreover, a high dry matter content effect on the relaxation was observed for sludge
380 samples and for sludge and wood mixtures. This effect was the same whatever the relaxation
381 time component, which confirmed that the dry matter content had the main effect on the NMR
382 parameters. Wood and sludge mixtures were scanned successfully by MRI using a spin echo
383 sequence. The grey level intensities were correlated with the dry matter content, thus
384 demonstrating the feasibility of MRI to quantify the water distribution in respiratory cells.
385 Moreover, image resolution was good enough for image analysis. Since voxel size was much
386 smaller than pore volume, porosity and specific surface area should be available.

387

388 **Acknowledgments**

389 The authors thank Mylene Launay and Mireille Cambert for their technical assistance.

390

391 **Figure legends**

392 Figure 1 **:** Diagram of respirometric apparatus
393

394 Figure 2 : Typical CPMG (a) and SR (b) decay curves for two ratios of sludge and wood with
395 70 % (■) and 24 % (♦) dry matter.

396

397 Figure 3 : Spin-spin relaxation time (T_2) distributions. Adjustments were made with the MEM
398 routine. (a) Sludge samples with 15%, 25% and 52% dry matter content (b) Wet wood with
399 dry mater of 45% (c) Mixtures of sludge and wood with 24.2%, 50.2% and 70.8% dry matter
400 content. One used the CPMG sequence (3000 echoes, with τ = 0.1 ms, RD = 2 s, NS = 8).

401

402 Figure 4 : Three component spin-spin relaxation rates ($1/T_2=R_2$) for (a) sludge samples and
403 (b) sludge and wood mixtures at various water over DM mass ratios. First component (◆),
404 second component (■) and third component (▲). One used the CPMG sequence (3000
405 echoes, with τ = 0.1 ms, RD = 2 s, NS = 8). Dashed lines $\propto(m_W/m_{DM})^{-1}$ are to assist reading.

406

407 Figure 5 : Spin-lattice relaxation time (T_1) distributions for mixtures of sludge and wood with
408 24.2% and 70.1% dry matter content (a). Adjustments were made with the MEM routine.
409 Three component spin-lattice relaxation rates (R_1) for sludge and wood mixtures at various
410 water over DM mass ratios (b). First component (◆), second component (■) and third
411 component (▲).One used the SR sequence (100 points with τ_1=5 ms, τ_{100}= 2000 ms, RD = 2
412 s, NS = 8). Dashed lines $\propto(m_W/m_{DM})^{-1}$to assist reading.

413

414 Figure 6 : Oxygen uptake rate over time for the two respirometric cells used in the combined
415 MRI-Respirometry set up.

Figure 7 : MRI images of respirometric cells 1 and 2 taken with a spin echo sequence (T_E = 8 ms, T_R = 1000 ms, FOV = 220 mm x 220 mm, thickness 2mm, sampling 256x256): Cell 1 at D0 (a) and D3 (b), Cell 2 at D0 (c) and D27 (d).MR images were representative of the area 3 cm below the centre of the airtight cylindrical reactor.

Figure 8 : Spin-spin relaxation intensities normalised by sample mass extracted from CPMG decay curves at 8 ms compared to dry matter content of sludge and wood mixtures. Samples were taken from the leftover mixture at D0 and at D3 and D27 from the respirometric cell 1 and cell 2, respectively. One used the CPMG sequence (3000 echoes, with tau=0.1ms, RD=2s, NS=8).

Figure 9 **:** MRI images of respirometric cell 2 at D27, taken with a spin echo sequence (TE = 8 ms, TR = 1000 ms, FOV = 220 mm x 220 mm, thickness 2mm, sampling 256x256). Selected images were separated by 3.6 cm. They are labelled from the bottom (slice 1) to the top (slice 45) of the cell.

References

Adani, F., Lozzi, P., Genevini, P., 2001. Determination of biological stability by oxygen uptake on municipal solid waste and derived products. Compost Science & Utilization 9, 163-178.

Agnew, J.M., Leonard, J.J., 2003. The physical properties of compost. Compost Science & Utilization 11, 238-264.

Annan, J.S., White, R.K. 1998 Evaluation of techniques for measuring air filled porosity in composts of municipal biosolids and wood chips. *In* Conference of composting in the southeast, September 9-11, Athens, Georgia, USA.

Araujo, C.D., Avramidis, S., Mackay, A.L., 1994. Behaviour of Solid Wood and Bound Water as a Function of Moisture Content a Proton Magnetic Resonance Study. Holzforschung 48, 69-74.

Araujo, C.D., Mackay, A.L., Hailey, J.R.T., Whittall, K.P., Le, H., 1992. Proton Magnetic-Resonance Techniques for Characterization of Water in Wood - Application to White Spruce. Wood Science and Technology 26, 101-113.

Belton, P.S. 1990 Can Nuclear Magnetic Resonance Give Useful Information About the State of Water in Foodstuffs? Comments on Agricultural and Food Chemistry Science 2,179-209..

Belton, P.S., Hills, B.P., 1987. The effects of diffusive exchange in heterogeneous systems on N.M.R line shapes and relaxation processes. Molecular Physics 61, 999-1018.

Berthe, L., Druilhe, C., Massiani, C., Tremier, A., de Guardia, A., 2007. Coupling a respirometer and a pycnometer, to study the biodegradability of solid organic wastes during composting. Biosystems Engineering 97, 75-88.

Bonn, D., Rodts, S., Groenink, M., Rafai, S., Shahidzadeh-Bonn, N., Coussot, P., 2008. Some applications of magnetic resonance imaging in fluid mechanics: Complex flows and complex fluids. Annual Review of Fluid Mechanics 40, 209-233.

Brownstein, K.R., Tarr, C.E., 1979. Importance of classical diffusion in NMR studies of water in biological cells. Physical Review A 19, 2446-2453.

Butz, P., Hofmann, C., Tauscher, B., 2005. Recent developments in noninvasive techniques for fresh fruit and vegetable internal quality analysis. Journal of Food Science 70, R131-R141.

Denisov, V.P., Halle, B., 2002. Hydrogen exchange rates in proteins from water H-1 transverse magnetic relaxation. Journal of the American Chemical Society 124, 10264-10265.

Duval, F., Cambert, M., Mariette, F., 2005. NMR study of tomato pericarp tissue by spin-spin relaxation and water self-diffusion. Applied Magnetic Resonance 28, 29-40.

Duval, F.P., Van Duynhoven, J.P.M., Bot, A., 2006. Practical implications of the phase-compositional assessment of lipid-based food products by time-domain NMR. Journal of the American Oil Chemists' Society 83, 905-912.

Faure, P., Care, S., Po, C., Rodts, S., 2005. An MRI-SPI and NMR relaxation study of drying-hydration coupling effect on microstructure of cement-based materials at early age. Magnetic Resonance Imaging 23, 311-314.

Gea, T., Barrena, R., Artola, A., Sanchez, A., 2004. Monitoring the biological activity of the composting process: Oxygen uptake rate (OUR), respirometric index (RI), and respiratory quotient (RQ). Biotechnology and Bioengineering 88, 520-527.

480 Grenier, A., Lucas, T., Collewet, G., Le Bail, A., 2003. Assessment by MRI of local porosity
481 in dough during proving. Theoretical considerations and experimental validation using
482 a spin-echo sequence. Magnetic Resonance Imaging 21, 1071-1086.
483 Gupta, R., Garg, V.K., 2008. Stabilization of primary sewage sludge during vermicomposting.
484 Journal of Hazardous Materials 153, 1023-1030.
485 Hartley, I.D., Kamke, F.A., Peemoeller, H., 1994. Absolute Moisture Content Determination
486 of Aspen Wood Below the Fiber Saturation Point Using Pulsed NMR. Holzforschung
487 48, 474-479.
488 Haug, R.T., 1993. The practical handbook of composting engineering. Lewis Publishers, Boca
489 Raton, Florida, USA.
490 Hills, B., 1998. Magnetic resonance imaging in food science. A Wiley Interscience
491 publication, New York. USA.
492 Hills, B.P., Takacs, S.F., Belton, P.S., 1989a. The effects of proteins on the proton NMR
493 transverse relaxation time of water. II protein aggregation. Molecular Physics 67, 919-
494 937.
495 Hills, B.P., Takacs, S.F., Belton, P.S., 1989b. The effects of proteins on the proton NMR
496 transverse relaxation times of water. I Native bovine serum albumine. Molecular
497 Physics 67, 903-918.
498 Hsi, E., Hossfeld, R., Bryant, R.G., 1977. Nuclear magnetic resonance relaxation study of
499 water absorbed on milled northern white-cedar. Journal of Colloid and Interface
500 Science 62, 389-395.
501 Iannotti, D.A., Grebus, M.E., Toth, B.L., Madden, L.V., Hoitink, H.A.J., 1994. Oxygen
502 Respirometry to Assess Stability and Maturity of Composted Municipal Solid-Waste.
503 Journal of Environmental Quality 23, 1177-1183.
504 Lens, P., Pol, L.H., Lettinga, G., Van As, H., 1997. Use of H^1 NMR to study transport
505 processes in sulfidogenic granular sludge. Water Science and Technology 36, 157-
506 163.
507 Lens, P., Vergeldt, F., Lettinga, G., Van As, H., 1999. H^1 NMR characterisation of the
508 diffusional properties of methanogenic granular sludge. Water Science and
509 Technology 39, 187-194.
510 Lucas, T., Grenier, A., Quellec, S., Le Bail, A., Davenel, A., 2005. MRI quantification of ice
511 gradients in dough during freezing or thawing processes. Journal of Food Engineering
512 17, 98-108.
513 Mantle, M.D., Sederman, A.J., 2003. Dynamic MRI in chemical process and reaction
514 engineering. Progress in Nuclear Magnetic Resonance Spectroscopy 43, 3-60.
515 Mariette, F., 2004. NMR relaxometry and MRI techniques: a powerful association in food
516 science. Comptes Rendus Chimie 7, 221-232.
517 Mariette, F. 2006 NMR imaging of dairy products. Modern Magnetic Resonance, Part 3:
518 Applications in Materials Science and Food Science, Springer; London, UK
519 Mariette, F., Guillement, J.P., Tellier, C., Marchal, P. 1996 Continuous relaxation time
520 distribution decomposition by MEM. *In* Signal Treatment and Signal Analysis in
521 NMR, Elsevier, Paris, France.
522 Marquardt, D.W., 1963. An algorithm for least squares estimations of nonlinear parameters.
523 Journal of the Society for Industrial and Applied Mathematics 11, 431.
524 Meiboom, S.G.D., 1958. Compensation for pulse imperfections in Carr-Purcell NMR
525 experiments. Review of Scientific Instruments 29, 688.
526 Menon, R.S., Mackay, A.L., Hailey, J.R.T., Bloom, M., Burgess, A.E., Swanson, J.S., 1987.
527 An NMR Determination of the physiological water distribution in wood during drying.
528 Journal of Applied Polymer Science 33, 1141-1155.

529 Muller, U., Bammer, R., Teischinger, A., 2002. Detection of incipient fungal attack in wood
530 using magnetic resonance parameter mapping. Holzforschung 56, 529-534.
531 Musse, M., Quellec, C., Devaux, M.F., Cambert, M., Lahaye, M., Mariette, F., 2009. An
532 investigation of the structural aspects of the tomato fruit by means of quantitative
533 nuclear resonance imaging. Magnetic Resonance Imaging 27, 709-719.
534 Olson, M.S., Ford, R.M., Smith, J.A., Fernandev, E.J., 2004. Quantification of bacterial
535 chemotaxis in porous media using magnetic resonance imaging. Environmental
536 Science & Technology 38, 3864-3870.
537 Palmowski, L., Müller, J., 2003. Anaerobic degradation of organic materials-significance of
538 the substrate surface area. Water Science and Technology 47, 231-238.
539 Richardson, J.C., Bowtell, R.W., Mader, K., Melia, C.D., 2005. Pharmaceutical applications
540 of magnetic resonance imaging (MRI). Advanced Drug Delivery Reviews 57, 1191-
541 1209.
542 Sherwood, J.L., Sung, J.C., Ford, R.M., Fernandez, E.J., Maneval, J.E., Smith, J.A., 2003.
543 Analysis of bacterial random motility in a porous medium using magnetic resonance
544 imaging and immunomagnetic labelling. Environmental Science & Technology 37,
545 781-785.
546 Snaar, J.E.M., Van As, H., 1992. Probing water compartments and membrane permeability in
547 plant cells by H^1 NMR relaxation measurements. Biophysical Journal 63, 1654-1658.
548 Su, D., McCartney, D., Wang, Q., 2006. Comparison of free air space test methods. Compost
549 Science & Utilization 14, 103-113.
550 Tremier, A., de Guardia, A., Massiani, C., Paul, E., Martel, J.L., 2005. A respirometric
551 method for characterising the organic composition and biodegradation kinetics and the
552 temperature influence on the biodegradation kinetics, for a mixture of sludge and
553 bulking agent to be co-composted. Bioresource Technology 96, 169-180.
554 Van Dusschoten, D., De Jager, P.A., Van As, H., 1995. Extracting diffusion constants from
555 echo-time-dependent PFG NMR data using relaxation-time information. Journal of
556 Magnetic Resonance Series A 116, 22-28.
557 Xu, Y., Araujo, C.D., MacKay, A.L., Whittall, K.P., 1996. Proton spin-lattice relaxation in
558 wood - T-1 related to local specific gravity using a fast-exchange model. Journal of
559 Magnetic Resonance Series B 110, 55-64.
560 Ziegler, G.R., MacMillan, B., Balcom, B.J., 2003. Moisture migration in starch molding
561 operations as observed by magnetic resonance imaging. Food Research International
562 36, 331-340.
563
564
565
566
567
568
569

Figure 1

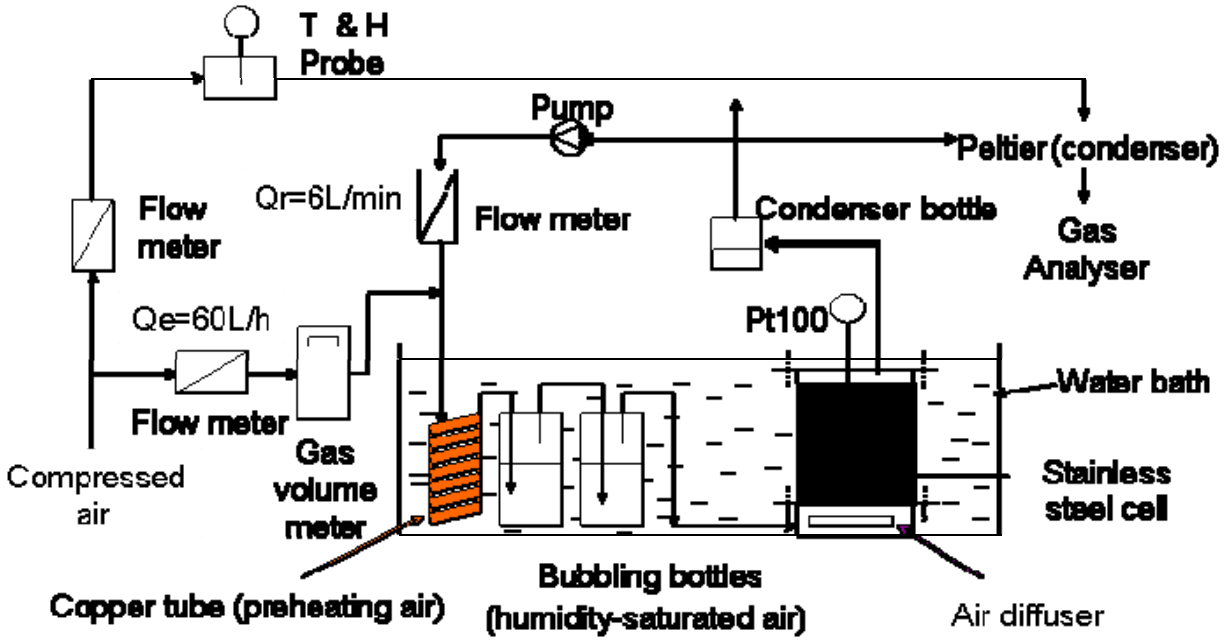

Figure 2

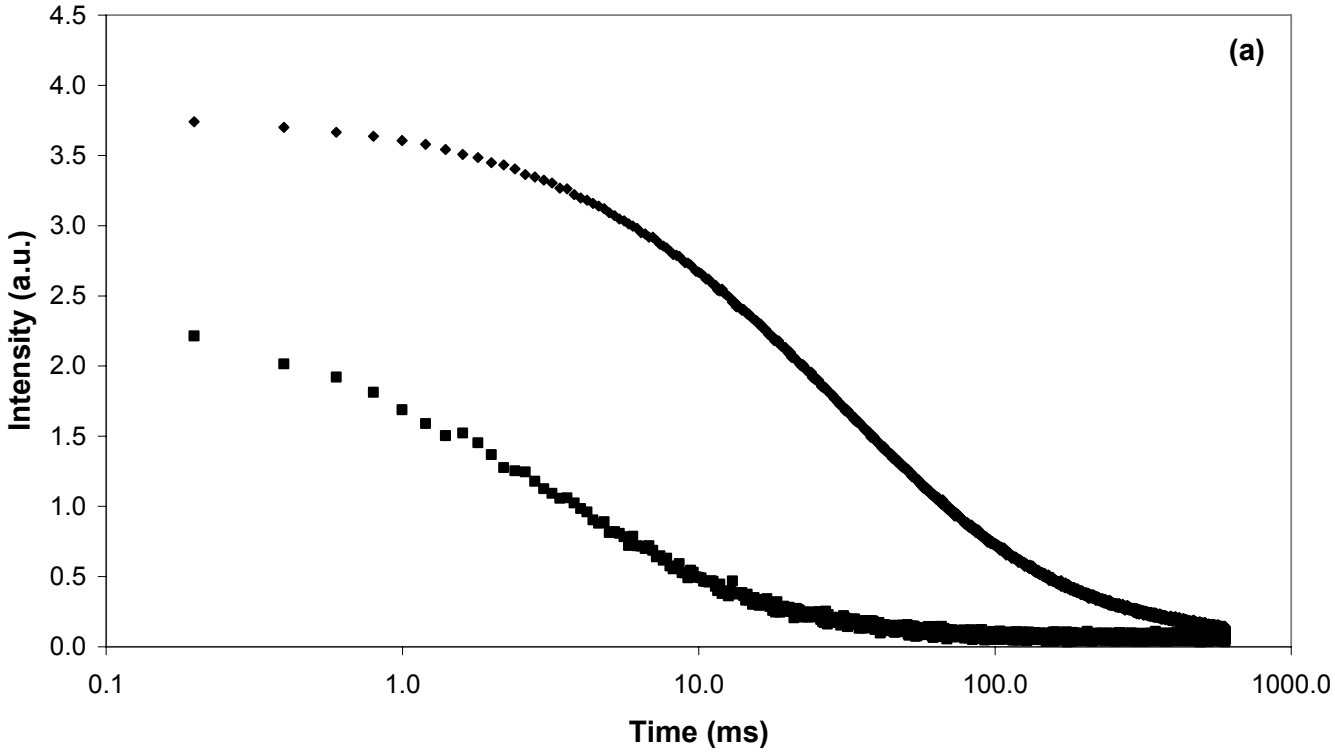

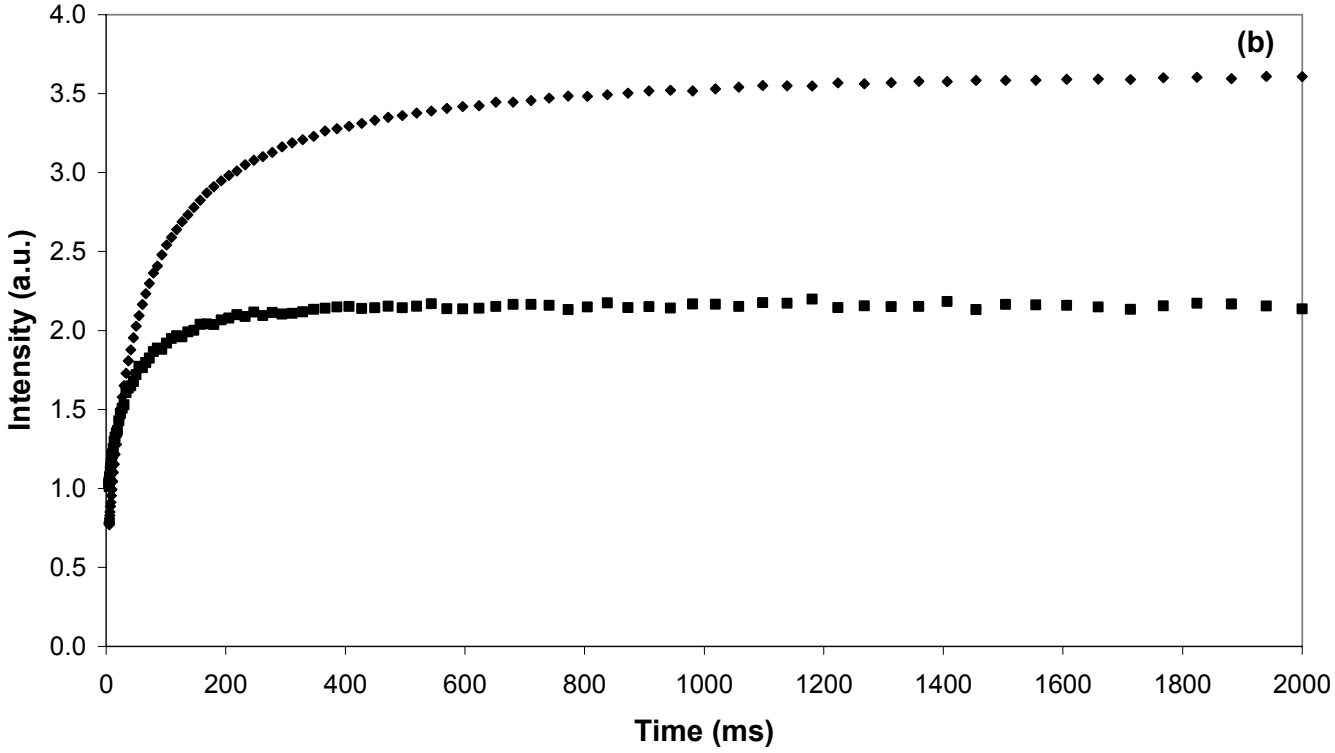

Figure 3

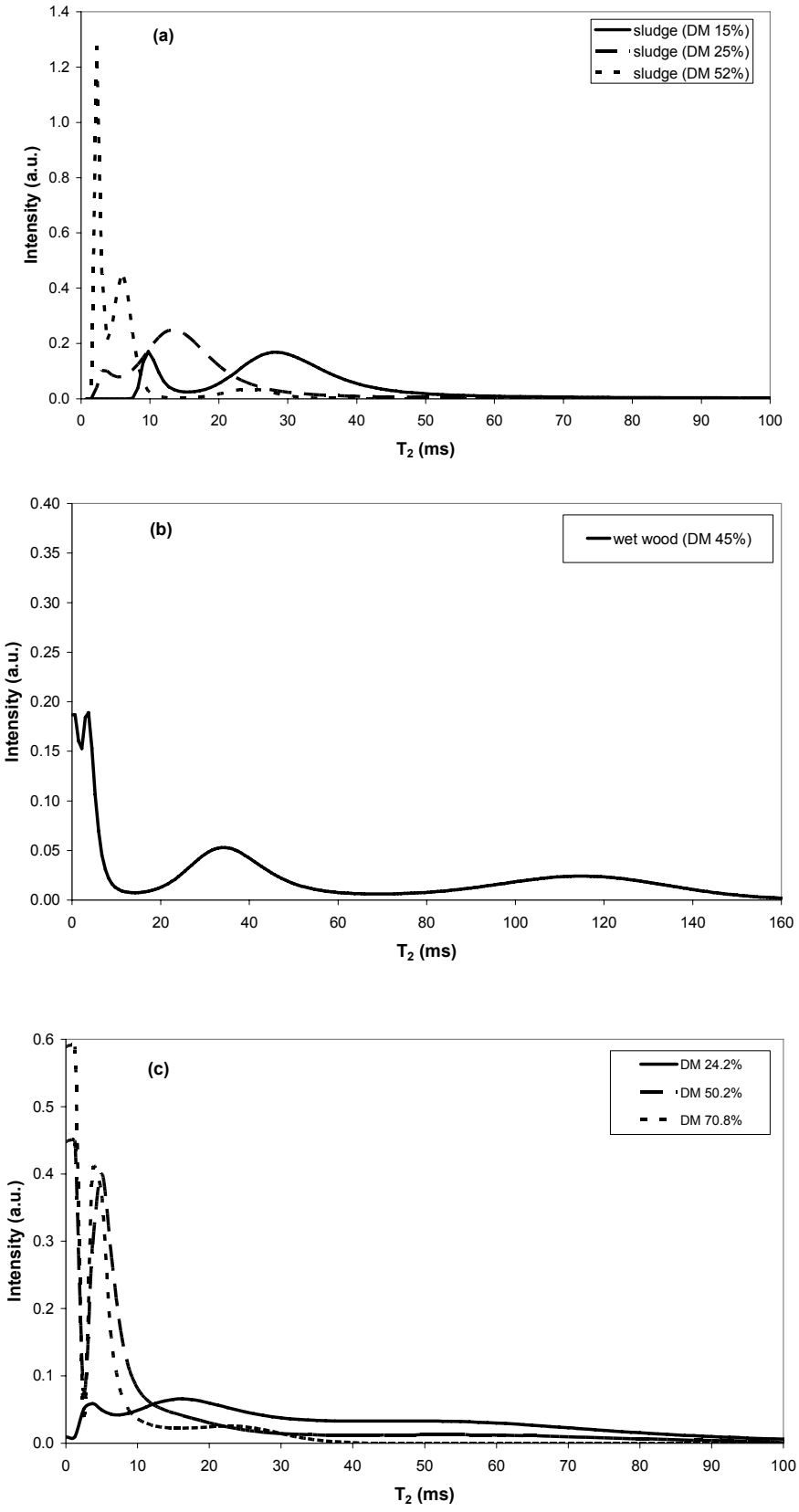

Figure 4

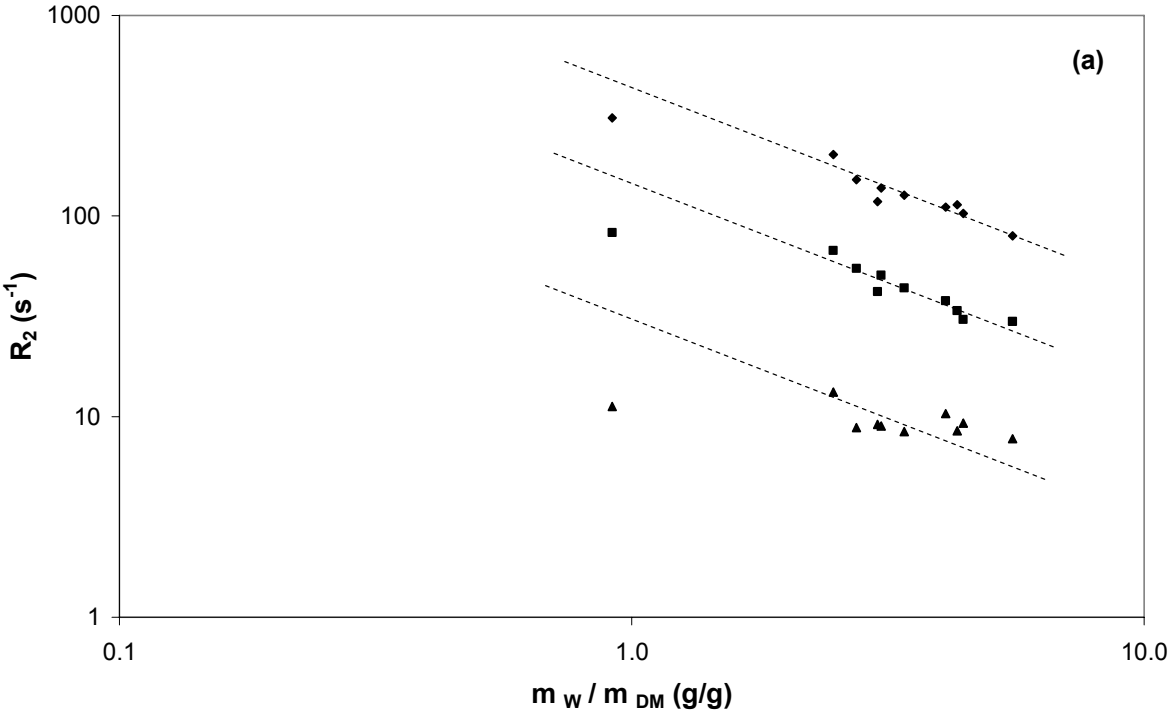

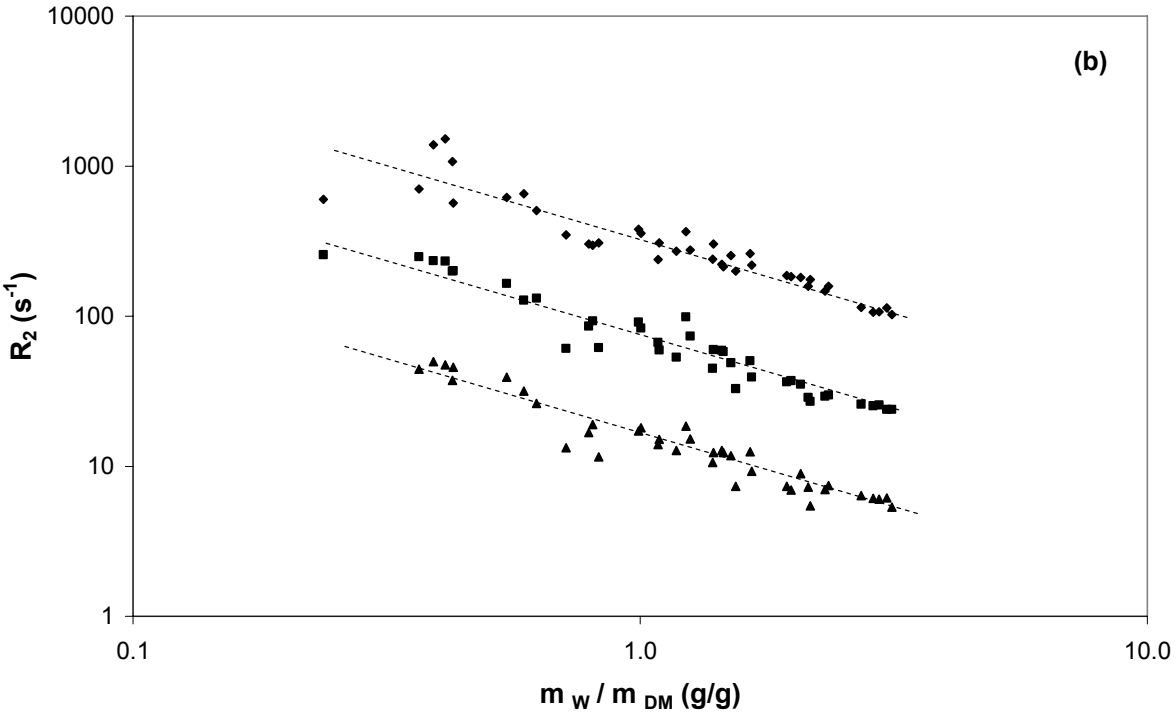

Figure 5

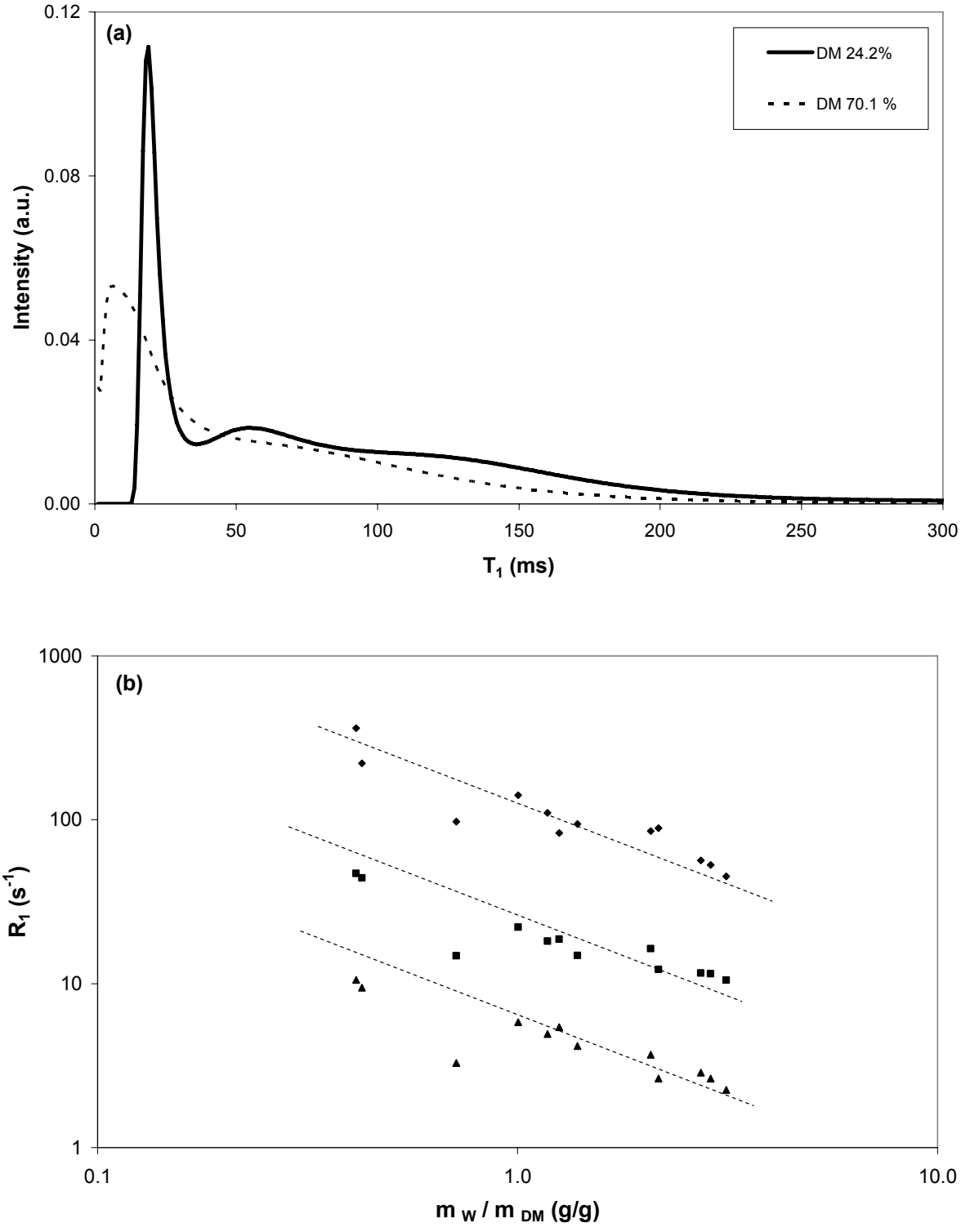

Figure 6

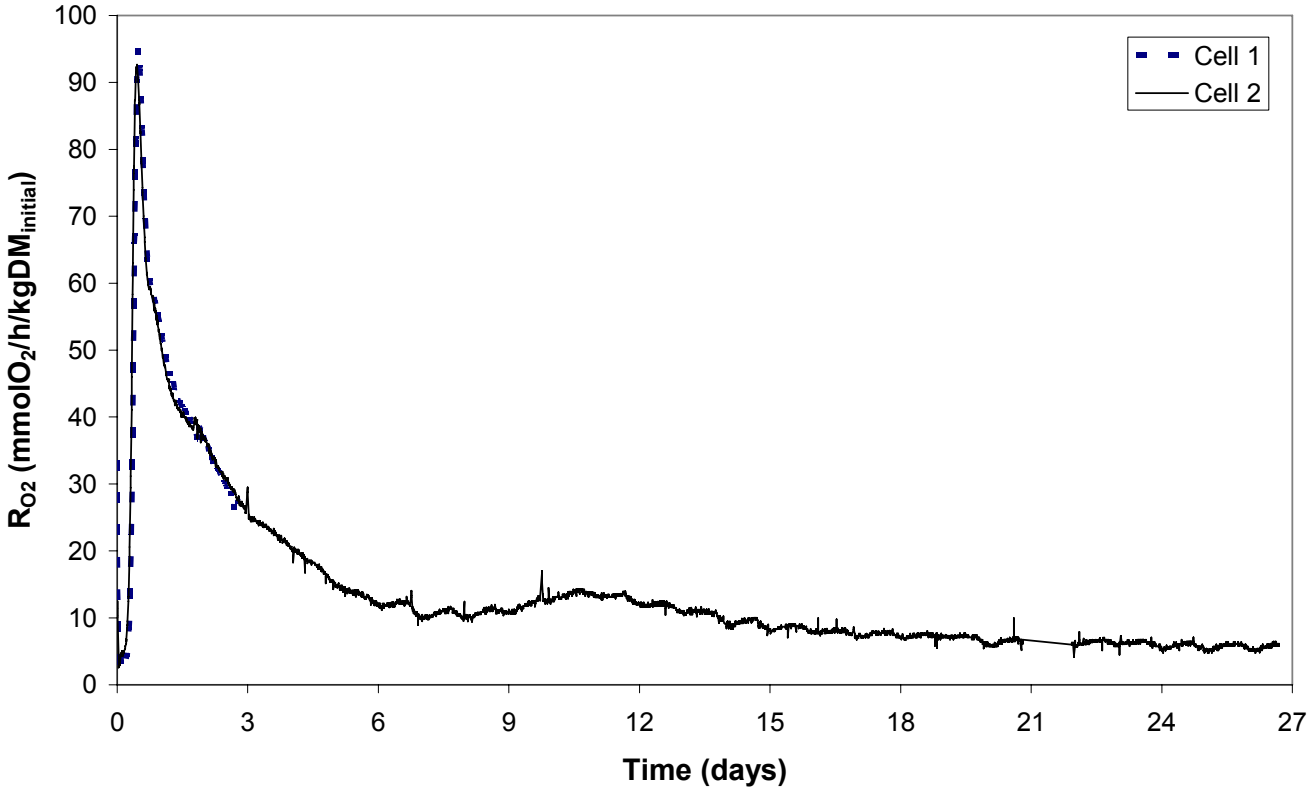

Figure 7

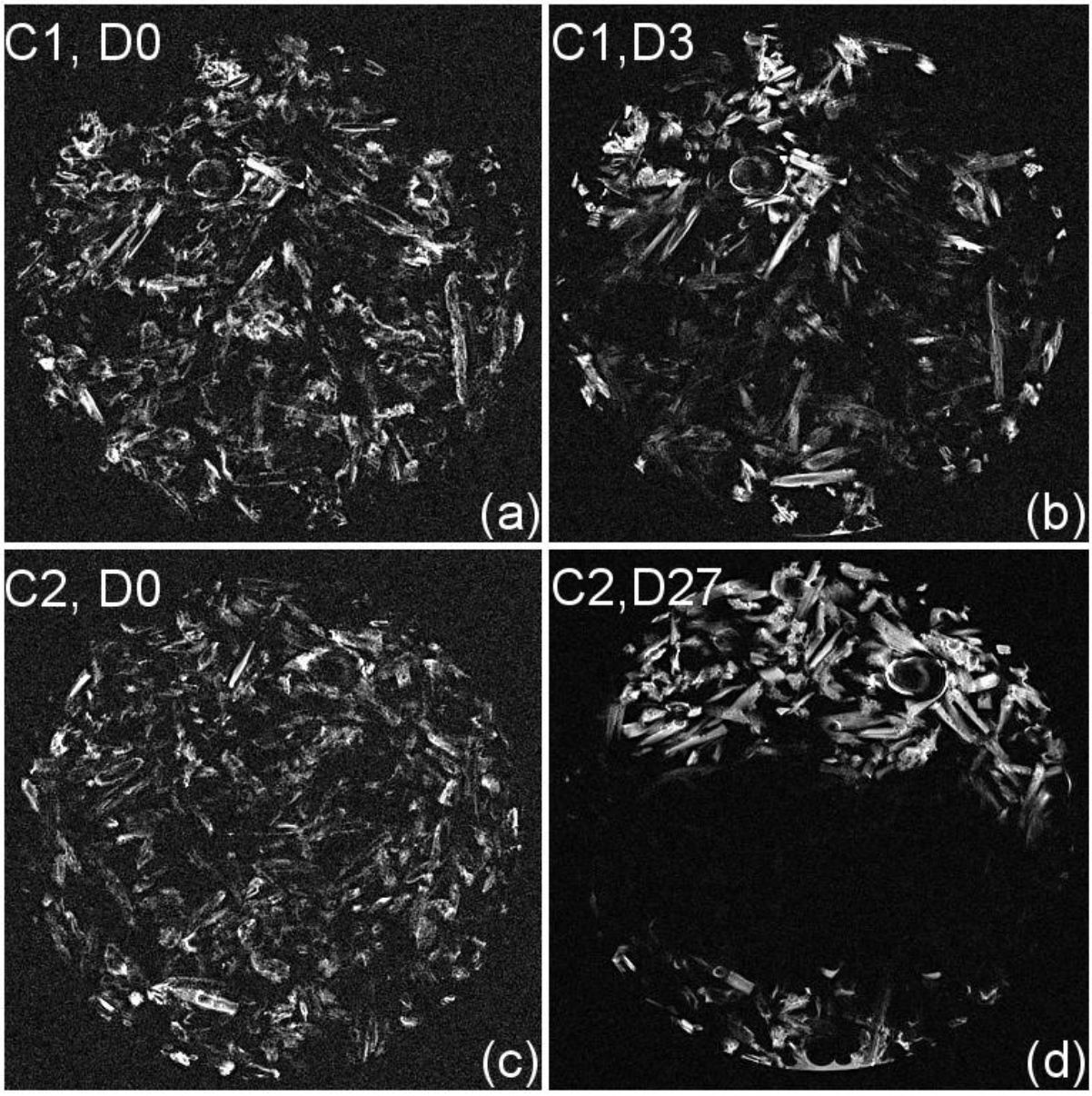

Figure 8

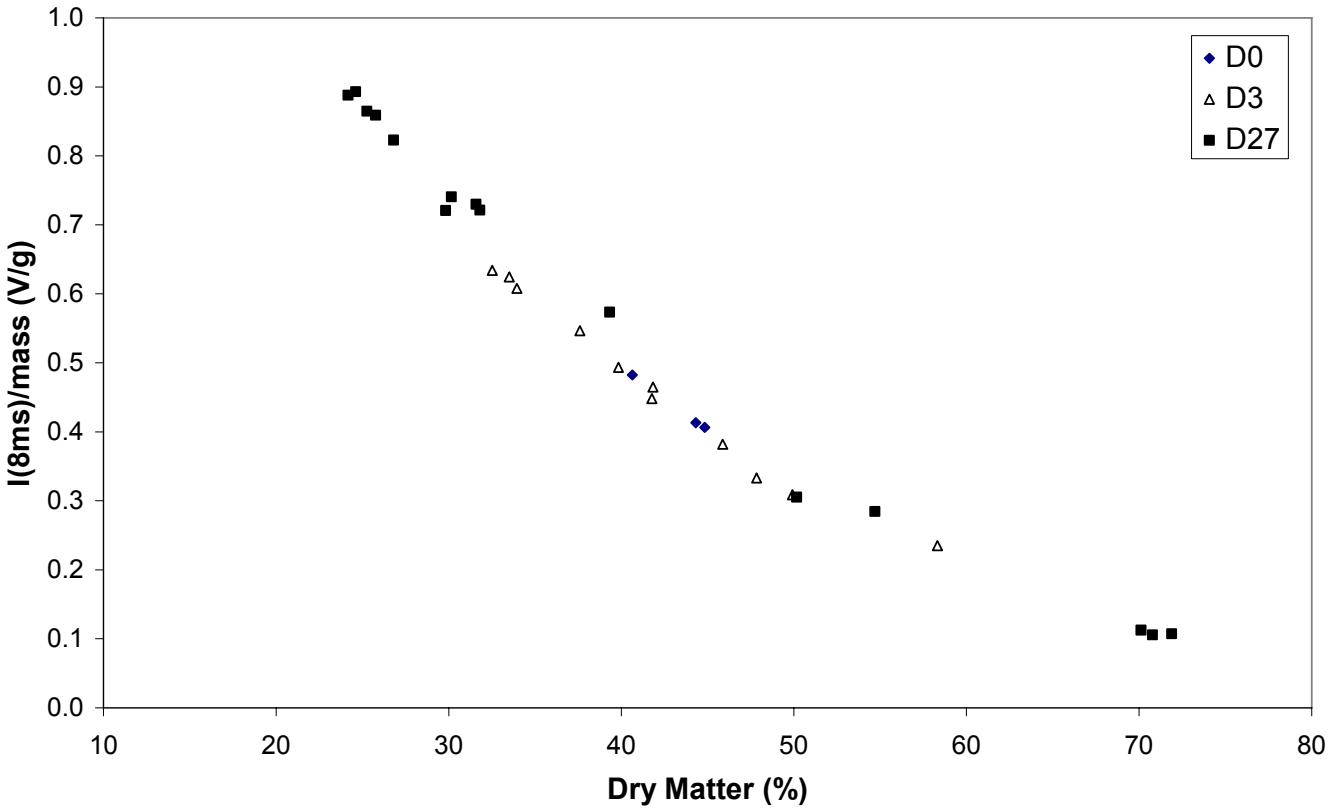

Figure 9